The Astrophysical Journal, 660: L73–L76, 2007 May 1

AEGIS: INFRARED SPECTRAL ENERGY DISTRIBUTIONS OF MIPS 70 μm–SELECTED SOURCES

M. Symeonidis,[1] D. Rigopoulou,[1] J.-S. Huang,[2] M. Davis,[3] M. L. N. Ashby,[2] P. Barmby,[2]
E. Egami,[4] G. G. Fazio,[2] E. Le Floc'h,[4] G. Rieke,[4] S. P. Willner,[2] and G. Wilson[5]
Received 2006 June 6; accepted 2006 November 17; published 2007 April 4

ABSTRACT

We present 0.5–160 μm spectral energy distributions (SEDs) of galaxies, detected at 70 μm with the Multiband Imaging Photometer for *Spitzer* (MIPS), using broadband imaging data from *Spitzer* and ground-based telescopes. Spectroscopic redshifts, in the range $0.2 \leq z \leq 1.5$, have been measured as part of the Deep Extragalactic Evolutionary Probe 2 (DEEP2) project. On the basis of the SEDs, we explore the nature and physical properties of the sources. Using the optical spectra, we derive Hβ and [O II]–based star formation rates (SFRs) that are 10–100 times lower than SFR estimates based on IR and radio. The median offset in SFR between optical and IR is reduced by a factor of ~3 when we apply a typical extinction correction. We investigate mid- to far-infrared correlations for low-redshift (>0.5) and high-redshift ($0.5 < z < 1.2$) bins. Using this unique "far-infrared"–selected sample, we derive an empirical mid- to far-infrared relationship that can be used to estimate the infrared energy budget of galaxies in the high-redshift universe. Our sample can be used as a template to translate far-infrared luminosities into bolometric luminosities for high-redshift objects.

Subject headings: galaxies: fundamental parameters — galaxies: high-redshift — infrared: galaxies

1. INTRODUCTION

The first breakthrough in infrared astronomy followed the launch of the *Infrared Astronomical Satellite*, which uncovered a substantial population of galaxies very luminous in the infrared (e.g., Neugebauer et al. 1984; Soifer et al. 1987). Its successor, the *Infrared Space Observatory*, demonstrated that a significant fraction of the energy budget in star-forming galaxies emerges in the infrared regime (e.g., Soifer et al. 1984). Since then, attempts to describe the nature of these objects have led to extensive studies of the properties of dust and its presence in star-forming regions, using spectral energy distributions (SEDs) and infrared colors as parameter constraints (e.g., Rowan-Robinson & Crawford 1989; Dale & Helou 2002). At the same time, correlations using photometry at different wavelengths have proved extremely useful in facilitating the study of the high-*z* universe and compensating for lack of long-wavelength infrared (IR) data (e.g., Sanders & Mirabel 1996).

Since the launch of the *Spitzer Space Telescope* (Werner et al. 2004), we are able to study the emission from interstellar dust across a wide range of environments both locally and at high redshifts. Deep surveys with the Infrared Array Camera (IRAC) and the Multiband Imaging Photometer for *Spitzer* (MIPS; Rieke et al. 2004) have provided a wealth of energy distributions at every redshift. This Letter presents the analysis of a sample of high-redshift sources detected at 70 μm by MIPS, in the region of the Extended Groth Strip (EGS). We have used a multitude of photometry in the near-, mid-, and far-infrared to construct SEDs and examine galaxy colors and have demonstrated the compatibility of this population with samples of local infrared luminous galaxies.

[1] Astrophysics Department, Oxford University, Oxford OX1 3RH, UK.
[2] Harvard-Smithsonian Center for Astrophysics, Cambridge, MA 02138.
[3] Department of Astronomy, University of California, Berkeley, CA 94720.
[4] Steward Observatory, University of Arizona, Tucson, AZ 85721.
[5] *Spitzer* Science Center, California Institute of Technology, Pasadena, CA 91125.

2. THE OBSERVATIONS

The All-Wavelength Extended Groth Strip International Survey (AEGIS) is a multiwavelength survey with a coverage of $2.0° \times 10'$ (Davis et al. 2007). MIPS observations of the EGS were conducted in two epochs: 2004 January and June. The effective EGS area with both IRAC and MIPS coverage is 725 arcsec^2. 180 70 μm sources were detected in this region with a point source sensitivity of 4 mJy at 5 σ (hereafter the MIPS 70 μm sample).

The IRAC and MIPS Basic Calibrated Data (BCD) delivered by the *Spitzer* Science Center included flat-field and linearity corrections, dark subtraction, and flux calibration. The BCD data were further processed by each team's own refinement routines, including distortion corrections, pointing refinement, mosaicking, and cosmic-ray removal by sigma clipping. We used DAOPHOT to extract sources from both IRAC and MIPS images; a point-spread function (PSF) FWHM of $1.8''$–$2.0''$ for IRAC and $35''/40''$ for MIPS 70 μm/160 μm was used. The aperture fluxes in each band were subsequently corrected to total fluxes using known PSF growth curves from Fazio et al. (2004) and Huang et al. (2004).

All 70 μm sources in the sample are detected at the IRAC 3.6, 4.5, 5.8, and 8.0 μm bands, and MIPS 24 μm bands. However, because of the different alignment of the MIPS and IRAC images, we do not have IRAC fluxes for all 70 μm sources. 88% of sources in the sample are also detected at 160 μm. In addition, the AEGIS data set (Davis et al. 2007) provides multiwavelength photometry and spectroscopic redshifts for the 70 μm sample, which permit the study of their X-ray-to-radio SEDs. 42 sources in the 70 μm population have a reliable DEEP2 spectroscopic redshift in the range of $0 < z < 1.2$ (we only use redshifts with qualities 3 or 4, according to the DEEP2 classification). We further divide the 70 μm sources in two redshift bins: $z \leq 0.5$ and $0.5 < z < 1.2$ (hereafter, "low" and "high" redshift). Although the DEEP2 project uses color criteria to preselect objects with photometric redshifts in the range 0.7–1.55, these constraints have not been imposed on the EGS; therefore, our redshift sample is not biased against the 70 μm sample. We limit the analysis in this Letter to 38 objects for which we have full visible-IR SEDs

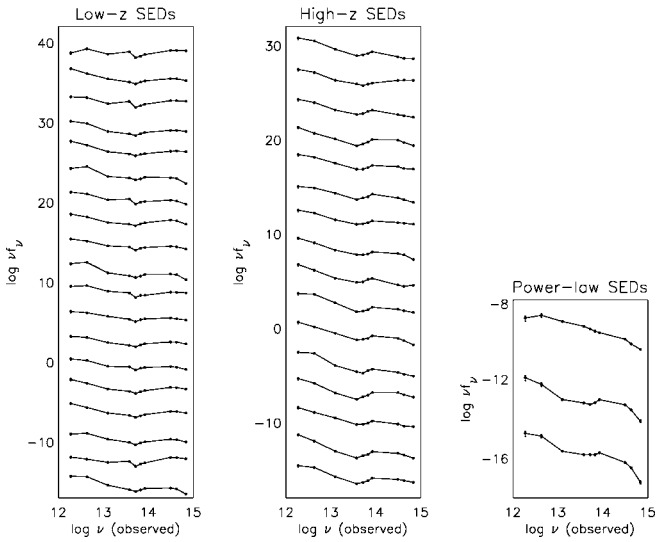

FIG. 1.—Full SEDs for the entire MIPS 70 μm sample with confirmed spectroscopic redshifts grouped into low-z (*left*), high-z (*middle*), and power-law (*right*) panels. The lower SED in each panel is in real y-axis units; for clarity, each subsequent SED in the low-z and power-law groups is transposed by 3 dex; in the high-z group the SEDs are transposed by 2 dex. In the direction of decreasing frequency, the 10 point photometry used to assemble the SEDs is: B, R, I magnitudes from CFHT, 3.6, 4.5, 5.8, and 8 m fluxes from IRAC and 24, 70, and 160 μm fluxes from MIPS.

and reliable (see above) spectroscopic redshifts (the remaining four objects do not have full SED coverage).

3. PROPERTIES OF THE 70 μm POPULATION

3.1. *Spectral Energy Distributions*

Using CFHT B, R, I imaging data and *Spitzer* photometry (3.6, 4.5, 5.8, 8.0, 24, 70, and 160 μm), we were able to construct 96 full SEDs, with 38 having reliable spectroscopic redshifts. The SEDs of all objects with reliable spectroscopic redshifts (38 sources) are shown in Figure 1. We group the SEDs in three panels: objects with low-z (*left*), high-z (*middle*), and a separate panel for objects with AGN-like SEDs (*right*).

Objects from the low-z/high-z groups show typical galaxy SEDs: the optical bands are dominated by starlight, which is then thermally reprocessed by dust and reemitted at longer wavelengths, giving rise to the noticeable increase in mid-infrared (MIR) flux. It is not surprising that the optical/near-IR part of the high-z SEDs is almost an order of magnitude lower than the low-z equivalent, as it samples a shorter wavelength region more strongly affected by extinction.

In the MIR regime (i.e., 12 μm $< \lambda <$ 24 μm) we find that the high-z objects have overall much higher flux densities than the low-z objects. There are two explanations for this: either high-z sources have higher hot dust emission shortward of 20 μm, or low-z sources have higher cold dust emission longward of 60 μm. Low-z objects show a predominant excess flux in the IRAC 8 μm band, which we attribute to emission at 6.2 and/or 7.7 μm, from polycyclic aromatic hydrocarbons.

In the far-infrared we note a large scatter in 160 μm fluxes evident in both low- and high-z sources. We find 70 μm/160 μm νf_ν ratios of ~1 and ~0.4 for the low- and high-z sources, respectively. This is in agreement with the energy distributions of local H II region–like galaxies (e.g., Dale et al. 2005, hereafter D05). In the *Spitzer* Infrared Nearby Galaxy Survey (SINGS) results, presented in D05, approximately 35% of the objects show a turnover at 160 μm, and their average $70\nu f_\nu/160\nu f_\nu$ ratios are ~1; accordingly, we evaluate our objects to be equally "warm" to local sources.

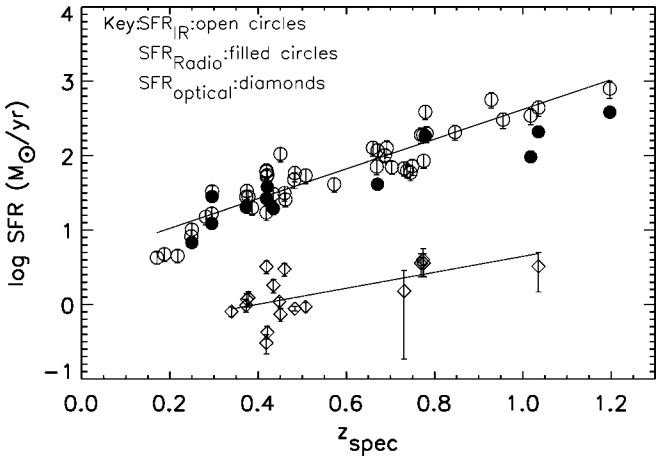

FIG. 2.—Plot of various indicators of the SFR as a function of redshift. SFRs estimated based on optical (Hβ and [O II]) emission lines (*open diamonds*), radio (*filled circles*), and IR (*open circles*) luminosities. The line fits represent the mean SFR_{IR} and SFR_{opt}.

Overall, the majority of our objects have characteristics consistent with those of luminous star-forming infrared galaxies. However, a small fraction (nine of 96) reveal power-law–type SEDs indicative of the presence of an active galactic nucleus (AGN; of the nine AGN candidates, only three have secure DEEP2 spectroscopic redshifts). These power-law–type sources have distinctly redder IRAC colors and are clearly identified in IRAC color plots. Interestingly, the available optical spectra do not show any of the characteristic signatures of an AGN, such as broad wings in the Balmer/oxygen lines; it is only with the addition of MIR data that we are able to peer through the obscuring dust and reveal the active nucleus. Only $\frac{1}{3}$ of these candidate AGNs are also detected in the X-rays, not surprising, as the *Chandra* full band (0.5–10 keV) data (flux limit 3.5×10^{-15} ergs s^{-1} cm^{-2}; Georgakakis et al. 2007) are not as deep as the MIPS and IRAC detections. The selected fraction of power-law–type galaxies agrees with a similar study in Frayer et al. (2006). However, taking into account ultrahard (5–10 keV) X-ray fluxes and hardness ratios leads us to an upper limit of 15% of AGNs in the sample, consistent with the findings of

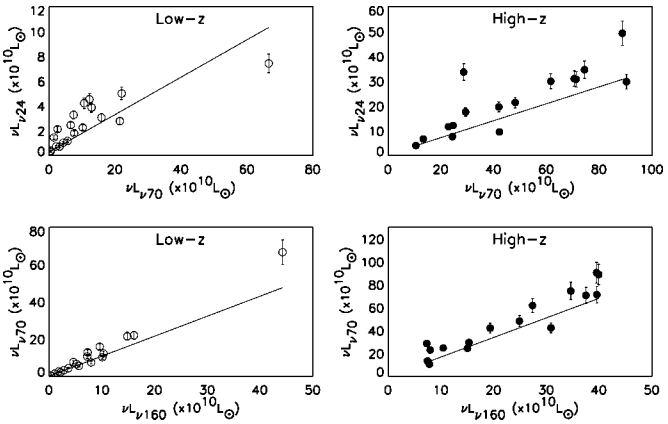

FIG. 3.—Linear mid- to far-infrared L_{24} vs. L_{70} and L_{70} vs. L_{160} luminosity correlations for the objects with spectroscopic redshifts. The two redshift bins are $z \leq 0.5$ (*open symbols*, *left*) and $z > 0.5$ (*filled symbols*, *right*). $\nu L_{\nu\lambda}$ represents the monocromatic luminosity of the objects at wavelength λ. The least square fit is shown for all four cases.

Fadda et al. (2002) and Franceschini et al. (2003). Brandt et al. (2006) show that in their 24 μm survey the contribution of AGNs is high (>40%) when selecting the brightest $z > 0.6$ sources, but ~10% when considering the whole redshift range. Our results are consistent with this study, as our power-law–type sources with spectroscopic redshifts are found at $z > 0.6$.

3.2. *Star Formation Rates*

In this section we carry out a comparative study of different diagnostics in order to trace the star formation rate (SFR) in our sample. Such a study is possible given the wealth of information available for the AEGIS project (Davis et al. 2007). We derive SFRs based on optical Balmer/[O II] emission lines, IR (present work), and 20 cm radio (Ivison et al. 2007) luminosities. Our computations are based on the prescriptions of Kennicutt (1983) and Bressan et al. (2002).

All available spectra were examined for the presence of hydrogen recombination and oxygen forbidden emission lines, as tracers of young stellar populations. We identified Hβ and [O II] features in 22% and 10% of the spectra, respectively. We extracted line fluxes by calibrating the continuum using CFHT optical/near-IR data and included stellar absorption corrections for each Balmer line. We derive an "average" $\mathrm{SFR_{opt}}$ of 2 $M_\odot$ yr^{-1}. Likewise, we derived average $\mathrm{SFR_{IR}}$ and $\mathrm{SFR_{radio}}$ of 100 and 80 $M_\odot$ yr^{-1}, respectively.

In Figure 2 we show a comparison of optical versus IR versus radio SFRs as a function of redshift for 38 objects from the 70 μm sample, which have full IRAC and MIPS photometry as well as reliable spectroscopic redshifts in the range $0 < z < 1.2$. Radio and IR SFRs reach values of ~900 $M_\odot$ yr^{-1}, revealing an active star-forming population. The $\mathrm{SFR_{IR}}$ is, on average, 50 times higher than the nonextinction-corrected $\mathrm{SFR_{opt}}$. Assuming an $A_V \sim 2$ (a typical A_V value for infrared-selected objects; see e.g., Rigopoulou et al. 2000), then $\mathrm{SFR_{IR}}/\mathrm{SFR_{optical}} \sim 10$ confirming that extinction is indeed very high. The fact that $\mathrm{SFR_{IR}} \sim \mathrm{SFR_{radio}}$ reinforces the notion that the 70 μm population is indeed made up of dusty star-forming galaxies. Moreover, it provides a nice confirmation that the radio–far-IR correlation that was found to exist for local galaxies (e.g., Condon et al. 1991) extends out to $z \sim 1$ sources. Finally, it is important to stress that any attempts to derive SFR estimates based on optical/UV measurements are likely to provide severe underestimates.

4. THE MID- TO-FAR-INFRARED CORRELATION

In this section we investigate the mid- to far-infrared luminosity correlations. We limit our study to objects with confirmed spectroscopic redshifts and full SEDs, and explore the correlations for each redshift bin separately. For our computations we have adopted a cosmology with $\Omega_M = 0.3$, $\Omega_\Lambda = 0.7$, and $H_0 = 71$ km s^{-1} Mpc^{-1}. Investigation of SEDs and behavior of colors (see earlier text) has led us to the conclusion that our 70 μm sample shares many similar characteristics with local infrared luminous galaxies. Consequently, to estimate *K*-corrections, we used the complete SED of the local galaxy NGC 4631 (convolved to the *Spitzer* resolution) and followed the prescription of Hogg et al. (2002). We are, of course, aware that use of a single template to derive *K*-corrections may introduce some biases. However, as Appleton et al. (2004) also point out, the presently available models do not fully encompass the observed parameters, especially in the far-infrared. This is likely to change with the availability of more *Spitzer* far-infrared data sets such as SINGS.

In Figure 3 we plot the 24 versus 70 and 70 versus 160 μm correlations. We have performed a weighted least-squares fit for each case, taking into account the calibration errors of 10% and 20% for the 24 and 70 μm fluxes, respectively, as well as the errors arising from SED fitting. We quantified the strength of the correlations using the Pearson linear coefficient. The Pearson coefficient ranges between 0 and $|1|$ for no or excellent correlation, respectively, with any intermediate value indicating the degree of linear dependence between the variables. Our values of ~0.8 for the 24–70 μm plot and ~0.9 for the 70–160 μm plot indicate a strong relation.

As expected, most of the energy in this population is emitted in the far-IR, also supported by the lines of best fit. By combining the above results, we derived a relationship to estimate the monochromatic luminosity at 160 μm from data at 24 and 70 μm, with an accuracy higher than 30%, for the low-*z* and high-*z* cases.

$$\text{For } z \leq 0.5: \quad L_{160} \sim 0.9L_{24} + 0.8L_{70} \quad (L_\odot), \tag{1}$$

$$\text{For } z > 0.5: \quad L_{160} \sim 0.6L_{24} + 0.4L_{70} \quad (L_\odot). \tag{2}$$

It is evident that the well-studied mid- to far-infrared relation found to hold for local galaxies (e.g., Dale & Helou 2002) can also be extended to the nonlocal universe. Although by limiting our study to the objects with spectroscopic redshifts we select in favor of the brightest sources, we still manage to sample a wide range of luminosities representative of $z \sim 1$ populations emerging through various deep infrared surveys. The correlations we have found can be used to obtain a direct estimate of the far-infrared luminosity of $z \sim 1$ objects and avoid the large errors introduced from mid- to far-infrared extrapolations of various galaxy templates.

M. S. has been supported by a Marie Curie Excellence Grant while working on this project, MEXT-CT-2003-002792. D. R. acknowledges support from the Leverhulme Trust via a Research Fellowship. This work is based on observations made with the *Spitzer Space Telescope*, which is operated by the Jet Propulsion Laboratory, California Institute of Technology, under NASA contract 1407. Support for this work was provided by NASA through contract 1256790 issued by JPL.

REFERENCES

Appleton, P. N., et al. 2004, ApJS, 154, 147
Brandt, K., et al. 2006, ApJ, 644, 143
Bressan, A., Silva, L., & Granato, G., L. 2002, A&A, 392, 377
Condon, J. J., Anderson, M. L., & Helou, G. 1991, ApJ, 376, 95
Dale, D. A., & Helou, G. 2002, ApJ, 576, 159
Dale, D. A., et al. 2005, ApJ, 633, 857
Davis, M., et al. 2007, ApJ, 660, L1
Fadda, D., Flores, H., Hasinger, G., Franceschini, A., Altieri, B., Cesarsky, C. J., Elbaz, D., & Ferrando, Ph. 2002, A&A, 383, 838
Fazio, G. G., et al. 2004, ApJS, 154, 39
Franceschini, A., et al. 2003, A&A, 403, 501
Frayer, D. T., et al. 2006, AJ, 131, 250
Georgakakis, A., et al. 2007, ApJ, 660, L15
Hogg, D. W., Baldry, I. K., Blanton, M. R., & Eisenstein, D. J. 2002, preprint (astro-ph/0210394)
Huang, J-S., et al. 2004, ApJS, 154, 44
Ivison, R. J., et al. 2007, ApJ, 660, L77
Kennicutt, R. C., Jr. 1983, ApJ, 272, 54

Neugebauer, G., et al. 1984, ApJ, 278, L1
Rieke, G. H., et al. 2004, ApJS, 154, 25
Rigopoulou, D., et al. 2000, ApJ, 537, L85
Rowan-Robinson, M., & Crawford, J. 1989, MNRAS, 238, 523
Sanders, D. E., & Mirabel, I. F. 1996, ARA&A, 34, 749
Soifer, B. T., Neugebauer, G., & Houck, J. R. 1987, ARA&A, 25, 187
Soifer, B. T., et al. 1984, ApJ, 278, L71
Werner, M. W., et al. 2004, ApJS, 154, 1